Effect of growth rate on the spatial distributions of dome-shaped Ge islands on Si(001)

Benjamin Cho, Thomas Schwarz-Selinger,* Kenji Ohmori, David G. Cahill,†
and J. E. Greene
Department of Materials Science and Engineering and the Frederick Seitz Materials Research Laboratory, University of Illinois, Urbana, Illinois 61801

(Received 26 April 2002; revised manuscript received 12 July 2002; published 14 November 2002)

Ge/Si(001) layers are grown by gas-source molecular beam epitaxy at 600 °C to probe island self-ordering phenomena. We vary the Ge growth rate by a factor of 40, 1.2–47 monolayers (ML) min^{-1}, and adjust the Ge coverage, 5.9–8.9 ML, to produce films consisting primarily of dome-shaped Ge islands. Measurements of the radial and nearest-neighbor distributions are compared to calculated distributions for random arrangements of circular islands. At low growth rates, island formation is inhibited at small separation. At high growth rates, the angular distributions of nearest-neighbor islands show pronounced island ordering along ⟨100⟩ directions.

DOI: 10.1103/PhysRevB.66.195407 PACS number(s): 68.55.−a, 81.16.Rf, 81.07.−b

I. INTRODUCTION

The growth of Ge/Si heterostructures has been intensely investigated in the recent past, due in large part to the fact that Ge/Si (4.2% lattice mismatch) serves as a model system for the study of lattice-mismatched heteroepitaxy. The strain-driven formation of three-dimensional coherent islands provides a method for the self-assembly of semiconductor nanostructures which have potential applications in novel device architectures.[1,2] In many of these applications, control of the surface spatial distributions of islands is essential. Frequently, the self-ordering of a single layer of islands is limited and therefore methods for enhancing island ordering are being vigorously studied—e.g., selective deposition,[3] templating by dislocation networks,[4] strain-driven pattern formation,[5,6] and multilayer growth.[7,8]

The evolution of islands morphologies in the Ge/Si(001) system at $T_s \approx 600$ °C is complex but the sequence of events is fairly well established. After the formation of a ≈3.5-monolayer (ML)-thick wetting-layer, island nucleation initially occurs via the formation of small two-dimensional (2D) islands which transform into 3D islands, ≈18 nm in diameter, with an aspect ratio of ≈0.04.[9] With continued Ge deposition, the small rounded islands quickly transform into square base pyramidal islands bounded by {105} facets. A fraction of these pyramidal islands, in turn, evolve[10,11] into coherent circular-base islands, with diameters of 45–100 nm and an aspect ratio of ≈0.2, which are commonly referred to as domes. Domes grow at the expense of pyramids.[10] Domes formed at a given set of growth conditions R, T_s, and layer thickness t tend to be quite uniformly sized in both lateral and vertical dimensions.[12,13] A fraction of the domes eventually relax by the introduction of dislocations and grow rapidly[14] to large sizes (>200 nm), forming ''superdomes.''

We focus our efforts on a fixed growth temperature and Ge coverage optimized for the formation of uniformly sized dome-shaped Ge islands. We analyze the effect of growth rate R on island size, areal density, nearest-neighbor position, and radial distribution functions. Sizes and areal densities of Ge islands[10,13,15–18] on Si(001) have been studied extensively but we are unaware of prior studies of the spatial distribution of Ge islands. [Nearest-neighbor angular[19] and radial[20] distributions have been reported for the related system InAs/GaAs(001).] In fact, quantitative data[21–24] for the spatial distribution functions of islands following film growth are relatively rare.

II. EXPERIMENTAL DETAILS

We use *n*-type Si(001) wafers with a miscut of ±0.25° and deposit Si buffer layers and Ge overlayers by gas-source molecular-beam epitaxy (GS-MBE) utilizing Si_2H_6 and Ge_2H_6 precursor gases in a multichamber ultrahigh vacuum (UHV) system. Following substrate cleaning,[15] degassing at 600 °C in UHV for >4 h, and flash heating to 1100 °C, we grow a 50-nm Si buffer layer at 800 °C, followed by Ge deposition at 600 °C. The growth rate R increases linearly with Ge_2H_6 flux[15] since $T_s = 600$ °C is far above the monohydride desorption temperature[25] for Ge(001) and the sticking coefficient[15,25] is constant at $S \approx 0.05$. The film thickness t required for obtaining a island population that is dominated by dome-shaped islands increases slightly with increasing R, from $t = 5.9$ ML at $R = 1.2$ ML min^{-1}, to $t = 8.9$ ML's at $R = 47.1$ ML's min^{-1}. The areal density of domes increases almost linearly with R and slowly with t.[9,15]

The growth temperature $T_s = 600$ °C is chosen to facilitate the formation of a narrow size distribution of domes while avoiding significant alloying[16] with the substrate. (At 550 °C domes coexist with a large population of pyramids.[15]) Our best evidence for the lack of alloying effects is the small variation in the size of domes with R; at $R = 0.4$ ML min^{-1} (15-min growth time), the dome size is essentially unchanged from $R = 1.2$ ML min^{-1} (5-min growth time). To increase the likelihood that our data are free of significant effects of intermixing with the substrate, we limit our analysis of the island distributions to $R > 1$ ML min^{-1}.

We measure Ge coverage by Rutherford backscattering spectrometry and image surface morphology by *ex situ* tapping-mode atomic force microscopy (AFM). We mount AFM specimens with the scan direction along [110] [see Fig. 1(a)] and measure island diameters from the resulting AFM images by reducing the vertical scale of the image to 2 nm, resulting in sharp contrast between the island perimeter and surrounding wetting layer. We then measure island height

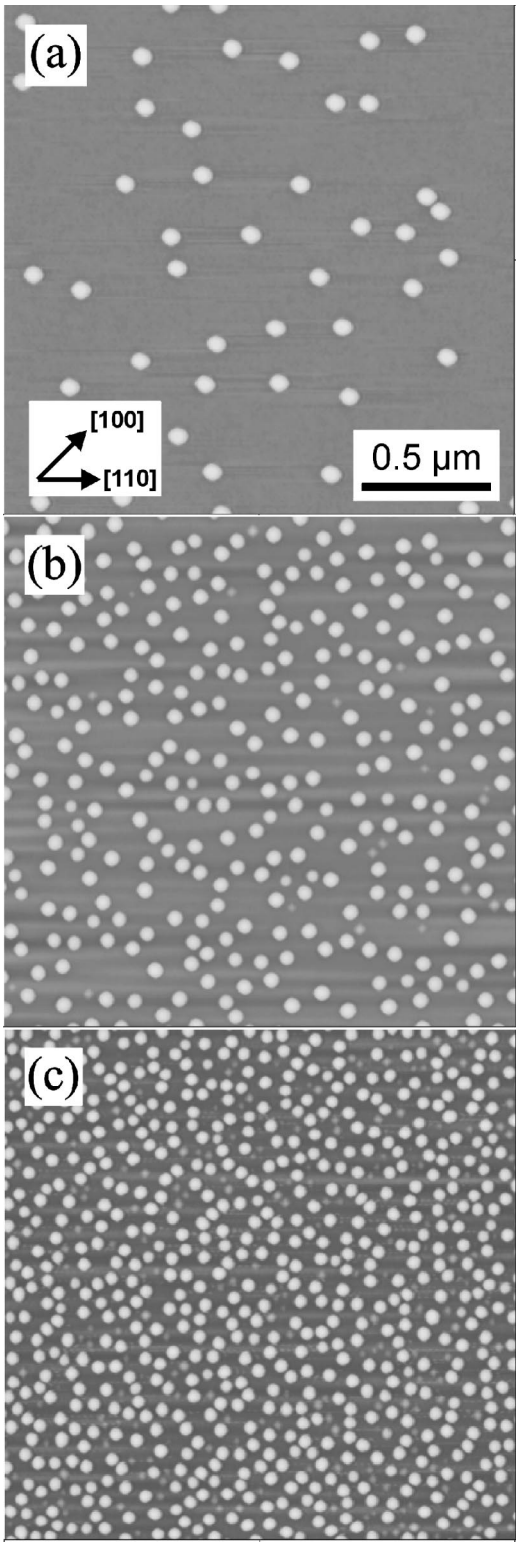

FIG. 1. 2×2 μm^2 AFM images of Ge/Si(001) layers grown at varying deposition rates R: (a) 1.2 ML min^{-1} with layer thickness $t=5.9$ ML and island area density $\rho=10.9$ μm^{-2}; (b) 6.6 ML min^{-1}, $t=8.0$ ML, $\rho=68.2$ μm^{-2}; (c) 47.1 ML min^{-1}, $t=8.9$ ML, $\rho=154.4$ μm^{-2}. Dome-shaped islands appear as light disks. Small pyramidal-shaped islands are visible in the background of (b) and (c).

referenced to the 2D wetting layer by analyzing a cross-sectional view of the same AFM image. From comparisons of island diameters measured from AFM images with those measured from plan-view TEM images,[12] we determine that our AFM measurements overestimate actual lateral dimensions by approximately 5 nm due to the effects of tip convolution.

We calculate nearest-neighbor distribution functions $N(r)$, radial distribution functions $G(r)$, and nearest-neighbor angular orientation functions $A(\theta)$ from the (x,y) coordinates of the center of each dome-shaped island. To determine the radial distribution $G(r)$, we use the coordinates (x_0,y_0) of a given island as a reference, and record the distance r from (x_0,y_0) to all neighboring islands within a given range (0.5 or 0.25 μm, depending on island density). The reference island position is chosen so that the measurement area does not intercept edges of the AFM image. Following the measurement, we take a new island position as the reference and repeat the process. The new reference island position is chosen at a sufficient distance from former reference positions to eliminate double counting. After performing a sufficient number of measurements (typically >3500 reference islands are needed to overcome statistical noise), we obtain the radial distribution function $G(r)$ by normalizing a histogram of all recorded separations by $2\pi sr\Delta r$, where s is the number of scans, r the distance from (x_0,y_0), and Δr the histogram bin size.

The nearest-neighbor distribution function $N(r)$ and angular distribution function $A(\theta)$ are determined in essentially the same manner as the radial distribution function, except we only consider the nearest-neighbor to a given reference island. We convert histograms of nearest-neighbor separation and angular orientation into the functions $N(r)$ and $A(\theta)$ by normalizing histogram values by $s\Delta r$ and $s\Delta r/2\pi$, respectively. Angular orientation measurements range from 0 to 2π, with 0 and π indicating alignment of islands along the horizontal axis of the 2D AFM image, and $\pi/2$ and $3\pi/2$ orientation indicating alignment along the vertical axis. Thus values of $\theta=0$, $\pi/2$, π, $3\pi/2$, and 2π correspond to $\langle 110\rangle$ directions, while $\theta=\pi/4$, $3\pi/4$, $5\pi/4$, and $7\pi/4$ correspond to $\langle 100\rangle$ directions.

We compare our experimental results to computer simulations of random nucleation that include the effects of an exclusion zones equal to the area of the island. (We note that analytical solutions of this problem can be derived in certain cases[26] but our computer simulations are flexible and simple to implement.) Using the average island diameter obtained from AFM measurements, we place circular islands one at a time in randomly generated locations. The only constraint on positioning is that island perimeters cannot overlap. If a newly determined random island position overlaps an existing island, we discard this position and generate another random (x,y) coordinate until one is found that does not result in overlap of an existing island. We repeat this process until the areal density of islands in the simulation matches the experimental value. We then determine $G(r)$ and $N(r)$ of these simulated island arrays in the same manner as described above. [The simulated $A(\theta)$ is constant.]

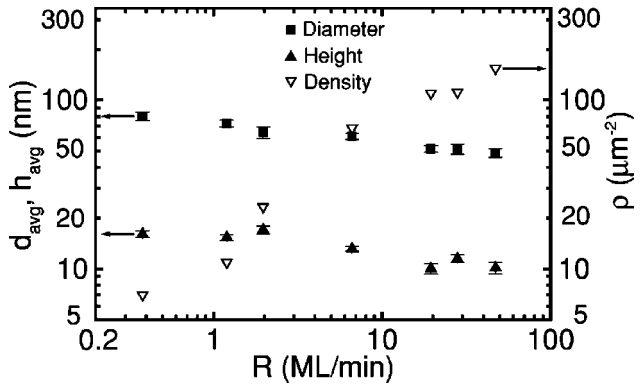

FIG. 2. Average height h_{avg}, diameter d_{avg}, and areal density ρ of Ge/Si(001) islands as a function of growth rate R. Error bars on h_{avg} and d_{avg} denote the standard deviation of the measurements.

III. RESULTS

Typical AFM images for films deposited at varying growth rate are shown in Fig. 1. By careful control over growth rate R and total amount of deposited material t, we are able to grow layers where the majority of islands are uniformly sized domes. Pyramidal islands are completely absent at the lowest growth rates. At the highest growth rates, a minority population of pyramids coexist with domes, see Fig. 1(c). A small change in coverage or growth temperature might alter the number of pyramids, but since the volume of Ge in the pyramids is a negligible fraction of the Ge volume in the domes, we do not believe that these residual pyramids significantly effect our results for the distributions of dome-shaped islands.

The effect of growth rate on island density ρ and island size is shown in Fig. 2. ρ increases with increasing R, ranging from $\rho=7$ at $R=0.4$ to $\rho=154.4\ \mu\text{m}^{-2}$ at $R=47.1$ ML's min^{-1}. The average dome diameter d_{avg} and height h_{avg} both decrease with increasing growth rate, with the diameter ranging from 73–48.7 nm and height from 16–10.1 nm as determined from AFM images. The distribution of island sizes is narrow; in most cases, the standard deviation of the height or diameter is $<7\%$.

Plots of $N(r)$ vs nearest-neighbor separation r_{nn} for experimental and simulated data are shown in Fig. 3. The experimental $N(r)$ are only slightly narrower than the simulations of random placement that include the effects of an exclusion zone. For our complete set of data for six growth rates, the peak in the experimental $N(r)$ is shifted to larger r_{nn} by $20\pm8\%$ relative to the peak in the simulated $N(r)$.

Radial distribution functions $G(r)$ for experimental and simulated data (solid lines) are shown in Fig. 4. $G(r)=0$ at $r<d_{avg}$ (the minimum center-to-center distance between islands is the island diameter) and approaches the area density ρ as $r\to\infty$. For $R<6.6$ ML min^{-1} ($\rho<68.2\ \mu\text{m}^{-2}$), the experimentally determined radial distribution functions increase monotonically with r, with the rate of increase slowly decreasing with increasing r as $G(r)\to\rho$. As the island density increases, so does the rate of increase in $G(r)$ observed at $r>d_{avg}$. However, the simulated $G(r)$ curves increase much more rapidly than the experimental data. This is most evident at low island density: the separation between the experimental and simulated curves is most significant at $\rho=10.9\ \mu\text{m}^{-2}$ ($R=1.2$ ML min^{-1}).

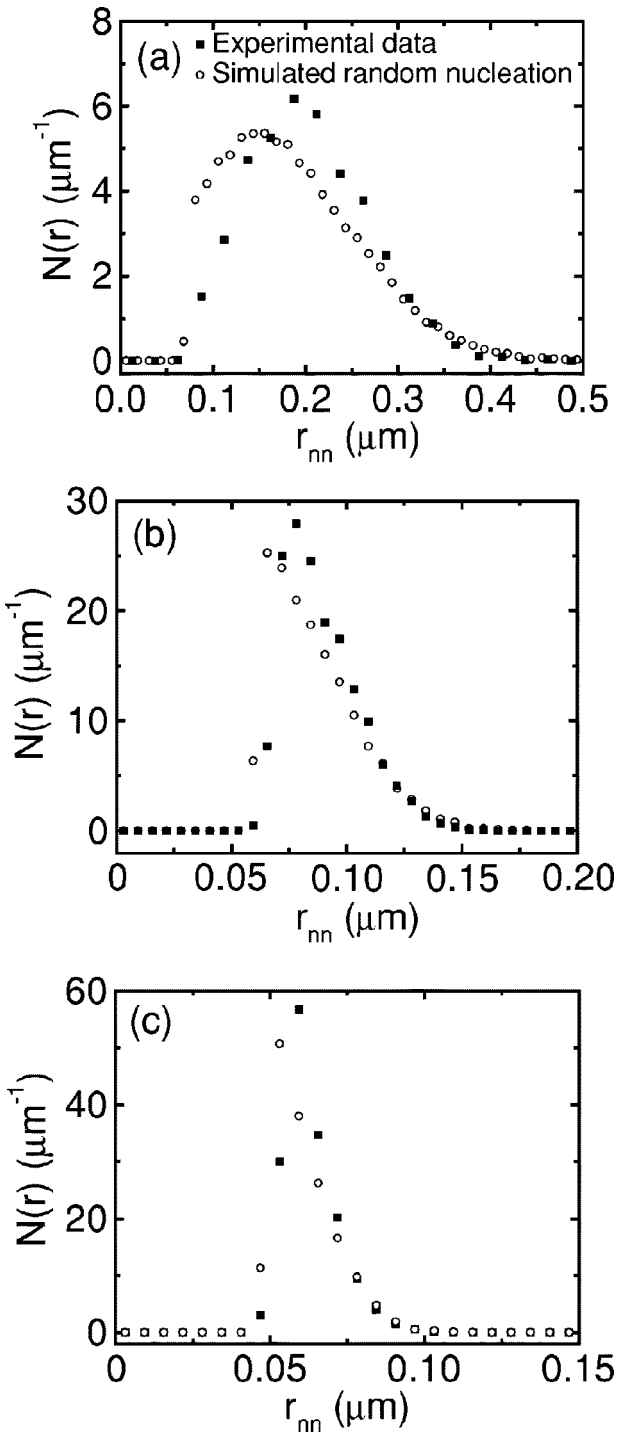

FIG. 3. (a)–(c) Filled symbols are the nearest-neighbor distribution function $N(r)$ plotted as function of the nearest-neighbor island separation r_{nn} for the Ge/Si(001) layers shown in Figs. 1(a)–(c), respectively. (Note that the scale of the x axis is different in each figure.) Open circles are $N(r)$ for computer simulations of the random placement of circular islands with an exclusion zone given by the measured average diameter of the islands.

The angular distribution function $A(\theta)$ for nearest-neighbor islands is shown in Fig. 5. At $\rho=10.9\ \mu\text{m}^{-2}$, no

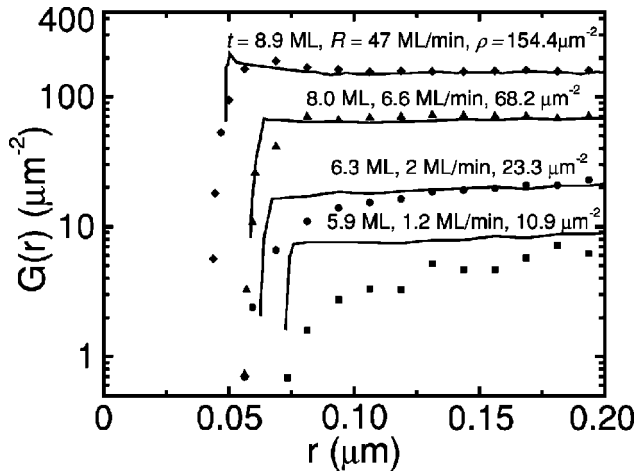

FIG. 4. Island radial distribution function $G(r)$ for experimental (filled symbols) and the simulated random placement of circular islands (solid lines). The experimental data are labeled by the coverage *t*, growth rate *R*, and island areal density ρ. The island areal density ρ also labels the simulated data.

preferential nearest-neighbor orientation is observed. As the island density increases, peaks appear in the $\langle 100 \rangle$ directions. The degree of ordering is particularly striking at the highest island density, see Fig. 5(c).

IV. DISCUSSION

We use the random placement of circular islands as a baseline for comparison with the experimental data. By including an exclusion zone equal in size to the measured average diameter of an island, we find reasonably good agreement between the simulations and the measured radial distributions of Ge dome-shaped islands; i.e., the measured radial distributions are approximately random. Island formation is inhibited, however, at small separations; this effect is seen in both $N(r)$ [the peak in $N(r)$ shifts to greater r_{nn}] and $G(r)$ [$G(r)$ is suppressed at small r]. The size of the excess excluded zone relative to the simulations is difficult to assign precisely but decreases from ≈ 40 nm at $R = 1.2$ ML min^{-1} to ≈ 25 nm at 2 ML min^{-1} to ≈ 7 nm at 47 ML min^{-1}, see Fig. 4.

Similar behavior is well known from studies of the deposition of noble metals on alkali-halide substrates.[23,24,27] In this case, the suppression of island nucleation at short distances is usually attributed to the capture zone of an island: the supersaturation of adatoms is reduced within a diffusion length of an existing island thus suppressing nucleation of new islands in the adjacent region. Our situation is complicated by the presence of the Ge wetting layer, shape transformations between pyramids and domes,[11] and ripening that occurs simultaneously with growth.[10] Nevertheless, we believe that the concept of a diffusion length is useful. The formation of dome-shaped islands is suppressed in a region surrounding an existing dome because the lower chemical potential of the elastically relaxed dome enables the dome to grow at the expense of the surrounding wetting layer and pyramids.

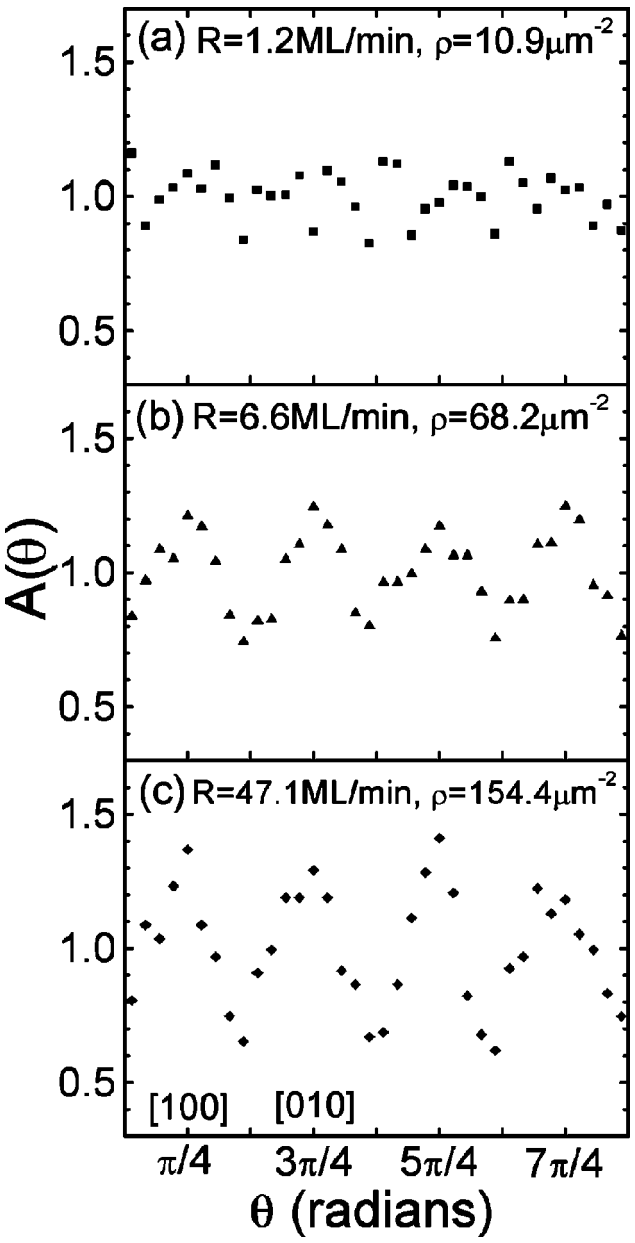

FIG. 5. (a)–(c) Angular distribution $A(\theta)$ of nearest-neighbor islands for the Ge/Si(001) samples shown in Figs. 1(a)–(c), respectively. The growth rate *R* and areal density of islands ρ are listed at the top of each figure.

The small length scale of the exclusion zones is somewhat surprising. We have recently studied denuded zones in Ge island densities on laser textured[28] Si(001) substrates; the size of the denuded zones adjacent to a vicinal surface is determined by the diffusion length during the time scale for the formation of the wetting layer.[15] The width of this denuded zone is, however, nearly 100 times the length of the exclusion zone discussed above. For example, at $R = 1.2$ ML min °C, the denuded zone adjacent to a vicinal surface is 4 μm wide.[15]

We can similarly discuss the increased degree of island ordering along $\langle 100 \rangle$ directions at high island densities in terms of surface mass transport. Meixner and co-workers[29]

have recently reported strong ⟨100⟩ ordering in $Si_{0.75}Ge_{0.25}$ islands grown by liquid phase epitaxy and attributed this ordering to anisotropic strain-induced modification of the surface chemical potential. Using numerical finite element calculations, they showed that the strain energy density for a pyramidal island has a local maximum near the island edge in the elastically hard ⟨110⟩ directions.[29] In contrast, the strain field in the ⟨100⟩ directions decays monotonically with distance from the island perimeter. At island boundaries, the elevated strain energy density in regions oriented along ⟨110⟩ directions effectively corresponds to regions of higher chemical potential than those oriented along ⟨100⟩. Thus mass transport is toward sites oriented in ⟨100⟩ directions relative to existing islands, and nucleation is suppressed in ⟨110⟩ directions.[29] Because of the short range of the strain fields (comparable to the island radius), this mechanism is enhanced at high island densities.

ACKNOWLEDGMENTS

The authors acknowledge the financial support of the U.S. Department of Energy (DOE), Division of Materials Sciences, under Contract No. DEFG02-91-ER45439, and the NSF Division of Materials Research Grant No. DMR 97-05440. Sample characterization by AFM, RBS, and TEM were performed at the Center of Microanalysis of Materials at the University of Illinois, which is partially supported by the DOE.

*Centre for Interdisciplinary Plasma Science, Max-Plank-Institut für Plasmaphysik, EURATOM Association, D-85748 Garching, Germany.

†Electronic address: d-cahill@uiuc.edu

[1] V.A. Shchukin and D. Bimberg, Rev. Mod. Phys. **71**, 1125 (1999).
[2] R. Loo, P. Meunier-Beillard, D. Vanhaeren, H. Bender, M. Caymax, W. Vandervorst, D. Dentel, M. Goryll, and L. Vescan, J. Appl. Phys. **90**, 2565 (2001).
[3] T.I. Kamins, R.S. Williams, and D.P. Basile, Nanotechnology **10**, 110 (1999).
[4] Y.H. Xie, S.B. Samavedam, M. Bulsara, T.A. Langdo, and E.A. Fitzgerald, Appl. Phys. Lett. **71**, 3567 (1997).
[5] J. Hong Zhu, K. Brunner, and G. Abstreiter, Appl. Phys. Lett. **73**, 620 (1998).
[6] P. Sutter and M.G. Lagally, Phys. Rev. Lett. **84**, 4637 (2000).
[7] F. Liu and M.G. Lagally, Surf. Sci. **386**, 169 (1997).
[8] J. Tersoff, C. Teichert, and M.G. Lagally, Phys. Rev. Lett. **76**, 1675 (1996).
[9] A. Vailionis, B. Cho, G. Glass, P. Desjardins, D.G. Cahill, and J.E. Greene, Phys. Rev. Lett. **85**, 3672 (2000).
[10] F.M. Ross, J. Tersoff, and R.M. Tromp, Phys. Rev. Lett. **80**, 984 (1998).
[11] F.M. Ross, R.M. Tromp, and M.C. Reuter, Science **286**, 1931 (1999).
[12] C.-P. Liu, P.D. Miller, W.L. Henstrom, and J.M. Gibson, J. Microsc. **199**, 130 (2000).
[13] T.I. Kamins, G. Medeiros-Ribeiro, D.A.A. Ohlberg, and R.S. Williams, J. Appl. Phys. **85**, 1159 (1999).
[14] J. Drucker, Phys. Rev. B **48**, 18 203 (1993).
[15] T. Schwarz-Selinger, Y.L. Foo, D.G. Cahill, and J.E. Greene, Phys. Rev. B **65**, 125317 (2002).
[16] S.A. Chaparro, Y. Zhang, J. Drucker, D. Chandrasekhar, and D.J. Smith, J. Appl. Phys. **87**, 2245 (2000).
[17] J.S. Sullivan, H. Evans, D.E. Savage, M.R. Wilson, and M.G. Lagally, J. Electron. Mater. **28**, 426 (1999).
[18] T.I. Kamins, E.C. Carr, R.S. Williams, and S.J. Rosner, J. Appl. Phys. **81**, 211 (1997).
[19] D. Bimberg, M. Grundmann, N.N. Ledentsov, S.S. Ruvimov, P. Werner, U. Richter, J. Heydenreich, Z.I. Alferov, P.S. Kop'ev, and V.M. Ustinov, Thin Solid Films **267**, 32 (1995).
[20] J.M. Moison, F. Houzay, F. Barthe, L. Leprince, E. André, and O. Vatel, Appl. Phys. Lett. **64**, 196 (1994).
[21] Y. Yang, Y.S. Luo, and J.H. Weaver, Phys. Rev. B **46**, 15 387 (1992).
[22] R.J. Barel, G.R. Carlow, M. Zinke-Allmang, Y. Wu, and T. Lookman, Physica A **239**, 53 (1997).
[23] H. Schmeisser, Thin Solid Films **22**, 99 (1974).
[24] J.C. Zanghi, J.J. Metois, and R. Kern, Philos. Mag. **29**, 1213 (1974).
[25] H. Kim, N. Taylor, J.R. Abelson, and J.E. Greene, J. Appl. Phys. **82**, 6062 (1998).
[26] V.I. Trofimov, Thin Solid Films **380**, 64 (2000).
[27] J.J. Metois, J.C. Zanghi, and R. Kern, Philos. Mag. **33**, 133 (1976).
[28] T. Schwarz-Selinger, D.G. Cahill, S.-C. Chen, S.-J. Moon, and C.P. Grigoropoulos, Phys. Rev. B **64**, 155323 (2001).
[29] M. Meixner, E. Schöll, M. Schmidbauer, H. Raidt, and R. Köhler, Phys. Rev. B **64**, 245307 (2001).